Anomalous thermal expansion, negative linear compressibility, and high-pressure phase transition in $ZnAu_2(CN)_4$: Neutron inelastic scattering and lattice dynamics studies

Mayanak K. Gupta,[1] Baltej Singh,[1,2] Ranjan Mittal,[1,2] Mohamed Zbiri,[3] Andrew B. Cairns,[4] Andrew L. Goodwin,[5] Helmut Schober,[3] and Samrath L. Chaplot[1,2]

[1]*Solid State Physics Division, Bhabha Atomic Research Centre, Mumbai 400085, India*

[2]*Homi Bhabha National Institute, Anushaktinagar, Mumbai 400094, India*

[3]*Institut Laue-Langevin, 71 avenue des Martyrs, Grenoble Cedex 9, 38042, France*

[4]*European SynchrotronRadiation Facility, BP 220, F-38043 Grenoble Cedex, France*

[5]*Department of Chemistry, University of Oxford, South Parks Road, Oxford OX1 3QR, United Kingdom*

(Received 6 June 2017; published 22 December 2017)

We present temperature-dependent inelastic-neutron-scattering measurements, accompanied by *ab initio* calculations of the phonon spectra and elastic properties as a function of pressure to quantitatively explain an unusual combination of negative thermal expansion and negative linear compressibility behavior of $ZnAu_2(CN)_4$. The mechanism of the negative thermal expansion is identified in terms of specific anharmonic phonon modes that involve bending of the -Zn-NC-Au-CN-Zn- linkage. The soft phonon at the L point at the Brillouin zone boundary quantitatively relates to the high-pressure phase transition at about 2 GPa. The ambient pressure structure is also found to be close to an elastic instability that leads to a weakly first-order transition.

DOI: 10.1103/PhysRevB.96.214303

I. INTRODUCTION

The discovery of large negative thermal expansion (NTE) in ZrW_2O_8 over a very broad temperature range triggered a keen interest in the field [1–13]. The NTE behavior was observed in several metal-oxide frameworks [11,14,15]. The observation of even larger NTE behavior in $Zn(CN)_2$ led to further impetus and discovery of NTE in a large number of cyanide compounds [3,16–24], e.g., $Cd(CN)_2$, $Ag_3Co(CN)_6$, $KMn[Ag(CN)_2]_3$, and MCN (M = Ag, Au, Cu).

Usually materials contract in all directions under hydrostatic pressure; however, there exists a small number of materials known to expand along specific directions [8,24–30]. This unusual pressure behavior, known as negative linear compressibility (NLC), is remarkably rare but has potential applications in high-pressure environments, such as optical telecommunication lines, shock absorbers, and highly sensitive pressure detectors. Both NLC and NTE are practically relevant to pressure-sensitive switches and temperature detectors for seismic, sonar, and aircraft applications. Compounds exhibiting these phenomena enter into the fabrication of incompressible as well as temperature-resistible composites of smart materials for next-generation body armor. There are very few attempts to address the possible mechanism that drives NLC behavior.

Large anisotropic behavior of elastic properties, negative Poisson's ratio, and NLC have been of particular interest in metal-organic frameworks. In this context, $ZnAu_2(CN)_4$ is known to exhibit NTE and exceptionally large NLC simultaneously [8,21]. The temperature dependence of the unit-cell parameters of $ZnAu_2(CN)_4$ (space group $P6_122$) indicates [8,21] that the thermal expansion is anisotropic and negative along the hexagonal c axis ($\alpha_a \sim 36.9 \times 10^{-6}\,K^{-1}$, $\alpha_c \sim -57.6 \times 10^{-6}\,K^{-1}$). The NLC along the c axis at ambient pressure is reported to be $\sim -42\,TPa^{-1}$, which is much larger than any other compound showing NLC behavior [8]. The compound has a large positive linear compressibility in the a-b plane which compensates the NLC along the c axis. The structure consists of molecular frameworks of $Zn(CN)_4$ units connected via Au atoms. The honeycomb structure of $ZnAu_2(CN)_4$ consists (Fig. 1) of polyhedral units and is believed to be responsible for its anomalous features. The compound also exhibits pressure-driven structural phase transition at $\sim$1.8 GPa [8]. The unit cell of the high-pressure phase is a $2 \times 2 \times 2$ supercell of the ambient pressure phase. The supercell implies that the transition may be driven by softening of an L-point phonon mode at the Brillouin zone boundary. This phase also shows NLC behavior along the c axis but with a lower magnitude in comparison to that of the ambient pressure phase.

Here we aim to understand the physics behind the rare and interesting combination of NTE and NLC in $ZnAu_2(CN)_4$, and its possible relation with the high-pressure transition, as well as to quantitatively explain these features. Since anharmonic phonons are expected to play a dominant role, we report detailed *ab initio* density-functional theory (DFT) calculations and temperature-dependent inelastic-neutron-scattering measurements of the phonon spectrum.

II. EXPERIMENTAL DETAILS

Inelastic-neutron-scattering measurements on about 1 cc of polycrystalline sample of $ZnAu_2(CN)_4$ were carried out on the direct-geometry cold-neutron time-of-flight time-focusing spectrometer IN6 at the Institut Laue Langevin (ILL, Grenoble, France). The spectrometer is equipped with a large detector bank covering a wide range of about 13° to 114° of scattering angle. Data were collected at 150, 225, 300, and 400 K, in the neutron energy gain setup and high-resolution mode, using an incident wavelength of 5.12 Å (3.12 meV). In the incoherent one-phonon approximation [31,32], the measured scattering function $S(Q, E)$, as observed in the neutron experiments, is related to the phonon density of states $g^{(n)}(E)$

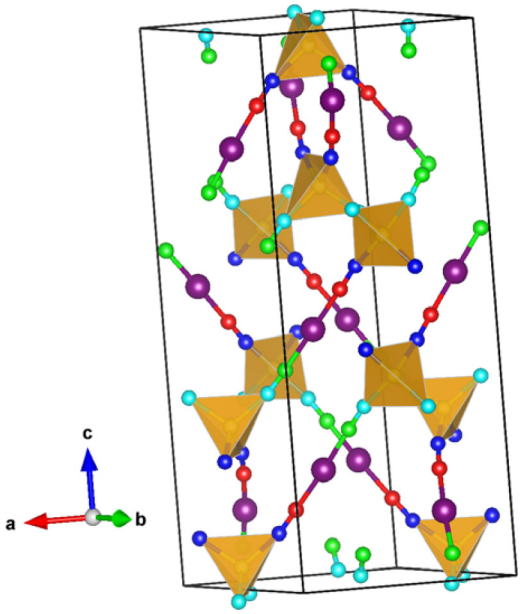

FIG. 1. Crystal structure of the ambient pressure phase of $ZnAu_2(CN)_4$. The c axis is along the chain direction, while the a- and b axes are in the horizontal plane. Zn atoms are at the center of tetrahedral units (yellow color). Key: C1, red sphere; C2, green sphere; N1, blue sphere; N2, cyan sphere; Au purple sphere; Zn, yellow sphere.

as follows:

$$g^{(n)}(E) = A\left\langle \frac{e^{2W(Q)}}{Q^2} \frac{E}{n(E,T) + \frac{1}{2} \pm \frac{1}{2}} S(Q,E) \right\rangle, \quad (1)$$

$$g^{n}(E) = B \sum_k \left\{ \frac{4\pi b_k^2}{m_k} \right\} g_k(E), \quad (2)$$

where the $+$ or $-$ signs correspond to energy loss or gain of the neutrons, respectively, and $n(E,T) = [\exp(E/k_BT) - 1]^{-1}$. A and B are normalization constants. b_k, m_k, and $g_k(E)$ are, respectively, the neutron-scattering length, mass, and partial density of states of the kth atom in the unit cell. The quantity between $\langle\,\rangle$ represents suitable average over all Q values at a given energy. $2W(Q)$ is the Debye-Waller factor averaged over all the atoms. The weighting factors $\frac{4\pi b_k^2}{m_k}$ in the units of barns/amu for Zn, Au, C, and N are 0.0631, 0.0394, 0.4625, and 0.8221, respectively. The values of neutron-scattering lengths for various atoms can be found from Ref. [33].

III. COMPUTATIONAL DETAILS

There are 66 atoms in the unit cell of $ZnAu_2(CN)_4$ in ambient phase, which gives 198 modes. The PHONON software [34] is used to estimate phonon frequencies in the entire Brillouin zone, as a subsequent step to density-functional theory total energy calculations using the VASP [35–37] software. The required force constants were computed within the Hellman-Feynman framework, on various atoms in different configurations of a supercell with ($\pm x$, $\pm y$, $\pm z$) atomic displacement patterns. An energy cutoff of 860 eV was used for plane-waves expansion. The Monkhorst-Pack method is used for k-point generation [38] and a $4 \times 4 \times 2$ k-point mesh was used. The exchange-correlation contributions were approximated using the generalized gradient approximation- Perdew Burke Ernzerhof functional [39,40]. The valence electronic configurations of C, N, Au, and Zn, as used in calculations for pseudopotential generation, are s^2p^2, s^2p^3, $d^{10}s^1$, and d^{10} p^2, respectively. The convergence breakdown criteria for the total energy and ionic loops were set to 10^{-8} and 10^{-5} eV Å^{-1}, respectively. Initially we have performed the optimization of the crystal structure with and without including the van der Waals interactions. The calculations show that inclusion of the van der Waals interaction produces the structure close to the experimental [8] values (Table I). The van der Waals (vdW) interaction has been included using the vdW-DFT method and using the optB88-vdW [41,42] functional.

The thermal expansion behavior has been computed under the quasiharmonic approximation. Each phonon mode of energy E_{qj} (jth phonon mode at point q in the Brillouin zone) contributes to the thermal expansion coefficient, which is given

TABLE I. Calculated and measured [8] structure and elastic properties of the ambient pressure phase of $ZnAu_2(CN)_4$.

		Expt. (x, y, z) $(T = 100$ K)	Calc. (x, y, z) $(T = 0$ K)
	a (Å)	8.3967	8.2096
	b (Å)	8.3967	8.2096
	c (Å)	20.9219	21.4616
C1	x	0.4020	0.4025
	y	0.2187	0.2189
	z	0.5289	0.5294
	u^2 (Å^2)	0.0131	0.0122 (100 K)
C2	x	0.2149	0.2128
	y	0.3985	0.3894
	z	0.3881	0.3879
	u^2 (Å^2)	0.0175	0.0124 (100 K)
N1	x	0.4455	0.4481
	y	0.1532	0.1570
	z	0.5697	0.5704
	u^2 (Å^2)	0.0131	0.0133 (100 K)
N2	x	0.7123	0.7145
	y	0.1491	0.1467
	z	0.6820	0.6808
	u^2 (Å^2)	0.0130	0.0132 (100 K)
Zn	x	0.5	0.5
	y	0	0
	z	0.6260	0.6261
	u^2 (Å^2)	0.0085	0.0081 (100 K)
Au	x	0.3164	0.3143
	y	0.3169	0.3133
	z	0.459	0.4593
	u^2 (Å^2)	0.0107	0.0103 (100 K)
	K_a (TPa^{-1})	52 (6)	62.5
	K_c (TPa^{-1})	−42(5)	−51.7
	B (GPa)	16.7(16)	13.6

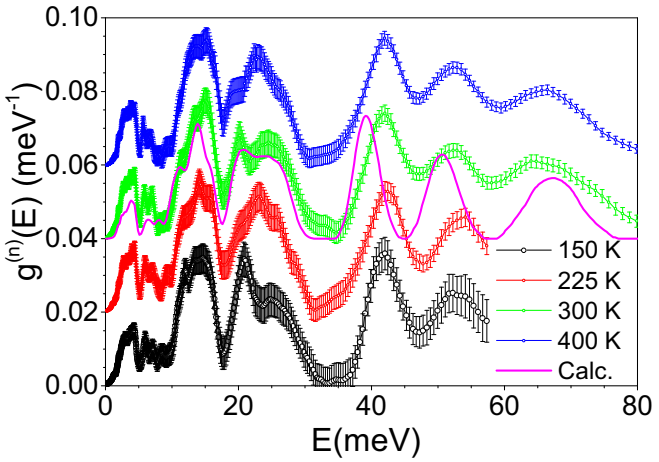

FIG. 2. Temperature-dependent inelastic-neutron-scattering spectra of the ambient pressure phase of $ZnAu_2(CN)_4$ along with the calculated neutron-weighted phonon spectrum.

by the following relation for a hexagonal system:

$$\alpha_a(T) = \frac{1}{V_0}\sum_{q,j} C_v(q,j,T)[s_{11}\Gamma_a + s_{12}\Gamma_b + s_{13}\Gamma_c], \quad (3)$$

$$\alpha_c(T) = \frac{1}{V_0}\sum_{q,j} C_v(q,j,T)[s_{31}\Gamma_a + s_{32}\Gamma_b + s_{33}\Gamma_c], \quad (4)$$

where V_0 is the unit-cell volume; Γ_a,Γ_b, and Γ_c are the anisotropic mode Grüneisen parameters. In a hexagonal system, Grüneisen parameters $\Gamma_a = \Gamma_b$. The mode Grüneisen parameter of phonon energy $E_{q,j}$ is given as [43]

$$\Gamma_l(E_{q,j}) = -\left(\frac{\partial \ln E_{q,j}}{\partial \ln l}\right)_{l'}; \quad l, l' = a, c. \quad (5)$$

Here s_{ij} are elements of elastic compliances matrix $s = C^{-1}$. $C_v(q,j,T)$ is the specific-heat contribution of the phonons of energy $E_{q,j}$ and given as

$$C_v(q,j,T) = E_{q,j} \times \frac{\partial}{\partial T}\left[\exp\left(\frac{E_{q,j}}{k_B T}\right) - 1\right]^{-1}. \quad (6)$$

The volume thermal expansion coefficient for a hexagonal system is given by

$$\alpha_V = (2\alpha_a + \alpha_c). \quad (7)$$

IV. EXPERIMENTAL AND CALCULATED PHONON SPECTRUM

The inelastic-neutron-scattering measurments are performed at various temperatures ranging from 150 to 400 K as shown in Fig. 2. The spectra show sharp peaks at about 4,7, 12, 22, 25, 42, 50, and 70 meV. Modes between 20 and 30 meV are subject to a significant change in energy as a function of temperature, indicating the anharmonic nature of these modes. The measured spectra at 150 and 225 K are shown only up to 55 meV due to the effect of the Bose-Einstein population factor affecting higher-energy phonons when cooling down. The energy of the C-N stretching mode is about 280 meV, which is not captured in the present measurements, using a cold-neutron spectrometer. Since thermal expansion and other thermodynamical properties are driven by low-energy modes, the measured spectral range is quite appropriate.

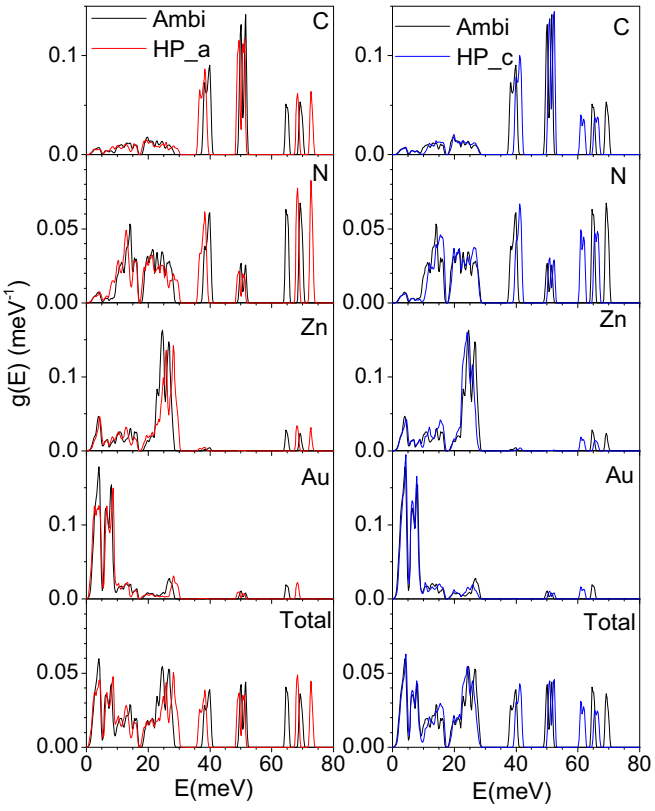

FIG. 3. Calculated partial density of states of various atoms of $ZnAu_2(CN)_4$ at ambient pressure, compared with anisotropic pressure along a and c axes. The cyanide stretch modes at about 280 meV are not shown.

Figure 3 shows the computed partial phonon densities of states of various atoms in this compound. These calculations reflect the atomic dynamics of individual atoms and their effect on properties of the compound. Vibrations of C and N atoms contribute to the entire spectral range, up to 280 meV, whereas Zn and Au atoms contribute up to 80 meV. However, the lower-energy spectra below 20 meV are largely dominated by heavier Au atoms.

The calculated neutron-weighted total phonon density of states is shown in Fig. 2. For clarity, the spectra are shifted vertically. It can be seen that the calculated density of states reproduces well the experimental spectrum. We note that Zn and Au do not contribute significantly to the total neutron-weighted density of states due to poor neutron cross section of these atoms (see Fig. 4). This indicates that dynamics of C and N atoms contribute the most to the measured neutron spectrum. The low-energy part below 30 meV has a major contribution from the N atom; however, both C and N contribute almost equally within the range 30–80 meV.

V. ANISOTROPIC THERMAL EXPANSION BEHAVIOR

The thermal expansion behavior of a compound arises from anharmonic atomic vibrations. It is expected that some of

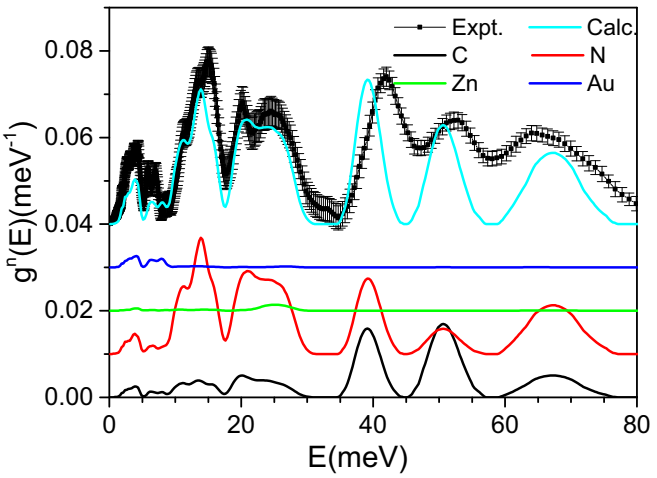

FIG. 4. Calculated neutron-weighted phonon spectra compared with measured inelastic spectra at $T = 300$ K, in the ambient pressure phase of $ZnAu_2(CN)_4$. The solid line with cyan color is the calculated total neutron-weighted phonon spectrum. The neutron-weighted partial density of states of C, N, Zn, and Au are shown by black, red, green, and blue solid lines, respectively.

the phonons contribute to NTE while others contribute to normal (positive) expansion of the material. The anomalous behavior can be understood by calculating the mode Grüneisen parameters and elastic compliance of the material (Table II).

We have calculated the anisotropic pressure dependence of phonon spectrum (Supplemental Material, Figs. S1 and S3 [44]). When the stress is applied, the maximum changes in the phonon spectra are observed above 20 meV. Interestingly, modes in the range 20–30 meV and above 60 meV behave differently than modes in the range 30–60 meV.

The Grüneisen parameters, Γ_a and Γ_c, due to change in lattice parameters "a" and "c," respectively, are shown in Fig. 5. The Grüneisen parameters show large negative values below 20 meV. The calculated linear thermal expansion coefficients at 300 K are $44 \times 10^{-6}\,K^{-1}$ and $-55 \times 10^{-6}\,K^{-1}$ along the a- and c axes, respectively (Fig. 6). The net volume thermal expansion coefficient is $33 \times 10^{-6}\,K^{-1}$ (Fig. 6). We have compared the experimentally measured [8,21] fractional change in lattice parameters and volume with our calculated results as a function of temperature (Fig. 7). We found that the calculated linear expansion along the a axis is in a good

TABLE II. Calculated elastic properties of the ambient pressure phase of $ZnAu_2(CN)_4$ as a function of pressure.

Compliance	0 GPa	1 GPa	1.5 GPa	2 GPa
s_{11} (TPa^{-1})	131.8	120.5	109.9	106.0
s_{33} (TPa^{-1})	62.5	31.8	23.7	19.5
s_{44} (TPa^{-1})	80.7	83.6	82.9	71.1
s_{12} (TPa^{-1})	−12.2	−35.8	−42.4	−49.0
s_{13} (TPa^{-1})	−57.1	−32.7	−24.31	−19.6
K_a (TPa^{-1})	62.5	52.1	43.2	37.4
K_c (TPa^{-1})	−51.7	−33.5	−24.9	−19.7
B (GPa)	13.6	14.16	16.25	18.2

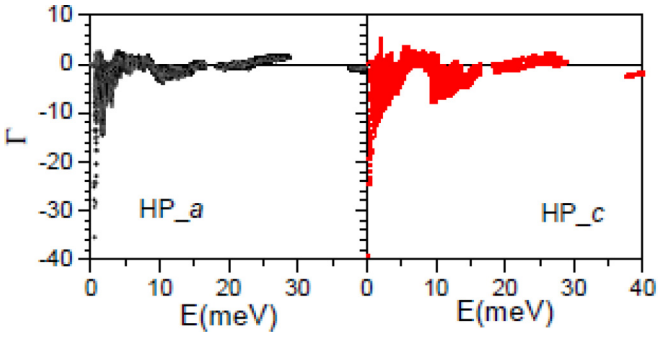

FIG. 5. Calculated Grüneisen parameters of $ZnAu_2(CN)_4$, Γ_a and Γ_c, averaged over the entire Brillouin zone on application of anisotropic pressure along the a axes (HP_a) and c axes(HP_c), respectively.

agreement with the measurements; however, along the c axis the calculations are slightly underestimated.

We have computed the linear thermal expansion coefficient as a function of phonon energy at $T = 300$ K (Fig. 8). It is interesting to see that modes which are contributing to the positive expansion in the a-b plane contribute to negative expansion along the c axis. This unusual behavior is attributed to large negative value of s_{13} (Table II) and hence related to NLC behavior of the compound. It suggests that any change in c axis would lead to change in the a axis in the opposite way. Hence, as temperature increases, the c axis decreases and expands the a axis. It is interesting to note that, although the anisotropic Grüneisen parameters are negative for compression along all the directions (Fig. 5), the combination of NLC and Grüneisen parameter leads to NTE (Fig. 7) only along the hexagonal axis.

The partial density of states of various atoms (Fig. 4) is used for the calculation of mean-squared displacements of various atoms (u^2) (Fig. 9) arising from all phonons of energy E in the Brillouin zone, as follows:

$$u^2(T) = \int \left(n + \frac{1}{2}\right) \frac{\hbar}{m_k E_{q,v}} g_k(E_{q,v}) dE_{q,v}, \qquad (8)$$

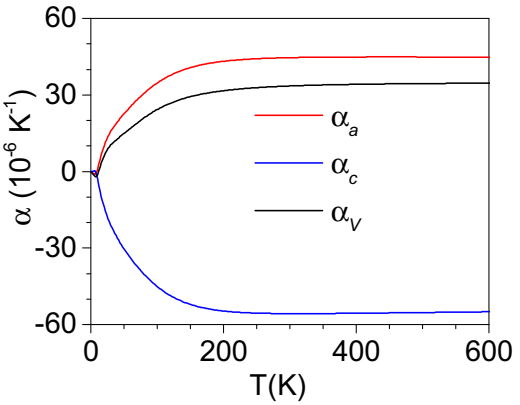

FIG. 6. Calculated linear and volume thermal expansion as a function of temperature in the ambient pressure phase of $ZnAu_2(CN)_4$.

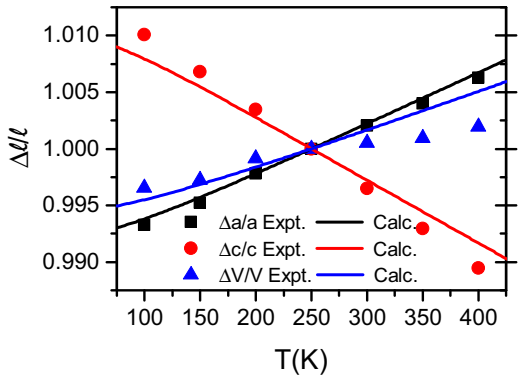

FIG. 7. Calculated and measured [21] fractional change in lattice parameters and volume as a function of temperature, in the ambient pressure phase of $ZnAu_2(CN)_4$.

where $n = [\exp(E_{q,v}/k_BT) - 1]^{-1}$; $g_k(E_{q,v})$ and m_k are the atomic partial density of states and mass of the kth atom in the unit cell, respectively.

The calculated mean-square displacement (u^2) of various atoms as a function of temperature is shown in Fig. 9(a). Usually, lighter atoms have larger mean-square displacement (u^2). However, our calculation shows that the u^2 value for Au atoms, which is the heaviest atom in the compound, is comparable with that of the lightest element, C. This suggests that the bonding of Au atoms with their neighboring atoms is highly flexible and provides enough flexibility to the structure for distortions required for NTE and NLC mechanism. Further, we have calculated the contribution to mean-square displacement from phonons of energy E at 300 K [Fig. 9(b)]. The mean-square displacement of all four atoms due to phonon energy below 5 meV is very large and dominated by Au atoms. The large amplitude of Au vibration will lead to bending of the -Zn-NC-Au-CN-Zn- chain and reduce the c dimension.

Since NTE behavior is largely determined by low-energy phonon modes, and also NLC is governed by the elastic constants which are related to the low-energy acoustic phonon modes, it seems then that the low-energy modes dominated by dynamics of Au atoms play a major role in these anomalous behaviors. We have identified a few phonon modes that contribute to anomalous thermal expansion behavior of $ZnAu_2(CN)_4$. The displacement pattern of such modes at high-symmetry points of the Brillouin zone are shown in Fig. 10. The modes can be better visualized by the animations which are available in the Supplemental Material [44]. The A-point mode of 1.3 meV ($\Gamma_a = 2.6$, $\Gamma_c = -12.7$) involves out-of-phase transverse vibrations of -Zn-NC-Au-CN-Zn- chains in the a-b plane. We find that modes at the Γ point (3.5 meV, $\Gamma_a = 2.2$, $\Gamma_c = -6.7$) and the K point (3.9 meV, $\Gamma_a = -2.1$, $\Gamma_c = -5.9$) involve out-of-phase translation motion and bending of -Zn-NC-Au-CN-Zn- chains. All these modes basically involve the transverse vibrations of -Zn-NC-Au-CN-Zn- chains and contribute to negative thermal expansion along the c axis and positive expansion in the a-b plane.

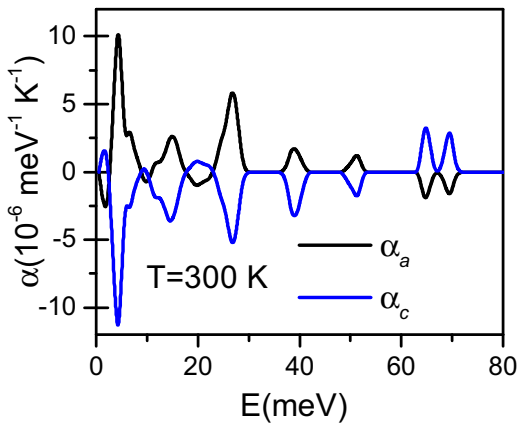

FIG. 8. Calculated contribution of various phonons of energy E to the linear thermal expansion along the a- and c axes at 300 K.

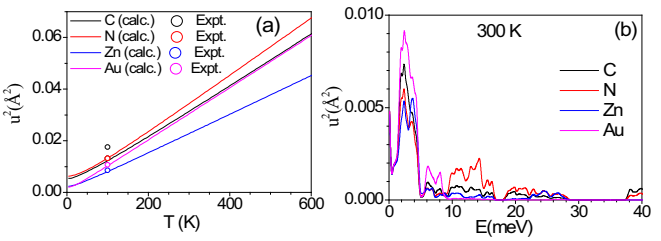

FIG. 9. (a) Calculated and experimental [8] mean-square displacement of various atoms in the ambient pressure phase of $ZnAu_2(CN)_4$. (b) Calculated mean-square displacement of various atoms as a function of phonon energy in the ambient pressure phase of $ZnAu_2(CN)_4$ at 300 K.

Analysis of the displacement pattern of these modes shows that all these modes involve perpendicular displacement of Au, C, and N atoms to the -Zn-NC-Au-CN-Zn- linkage. The magnitude of this displacement is largest for Au in these modes. These kinds of anharmonic modes bend the -Zn-NC-Au-CN-Zn- linkage and contract the c axis as well as expand the a-b plane.

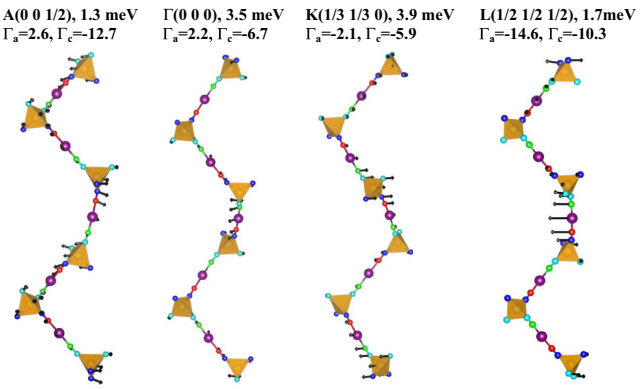

FIG. 10. Calculated eigenvectors of selected phonon modes in the Brillouin zone in the ambient pressure phase of $ZnAu_2(CN)_4$. The c axis is along the chain direction, while the a- and b axes are in the horizontal plane. Zn atoms are at the center of tetrahedral units (yellow color). Key: C1, red sphere; C2, green sphere; N1, blue sphere; N2, cyan sphere; Au, purple sphere; Zn, yellow sphere.

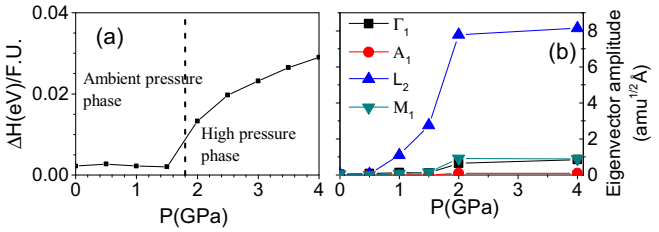

FIG. 11. (a) Calculated difference in enthalpy between the ambient and high-pressure phases, as a function of pressure. (b) Calculated distortion in terms of the amplitude of eigenvector of phonon modes as a function of pressure in the ambient pressure phase of $ZnAu_2(CN)_4$. The symbols represent the points at which calculations are performed.

VI. HIGH-PRESSURE PHASE TRANSITION

The compound $ZnAu_2(CN)_4$ is known to undergo a high-pressure structural transition at about 1.8 GPa [8]. The structure of the high-pressure phase (space group $P6_422$) is related to the $2 \times 2 \times 2$ supercell of the parent structure (space group $P6_222$). The high-pressure phase transition is reported to be displacive in nature [8]. The two phases are found to be related by rotations of the Zn-centered coordination tetrahedra [8]. The supercell implied that the transition may be associated with a soft phonon mode at the $L(1/2\ 1/2\ 1/2)$ point in the Brillouin zone of the parent structure (space group $P6_222$). The calculated pressure dependence of the phonon-dispersion relation shows a large softening of the L-point phonon mode (see Fig. S1 [44]), which supports the above argument.

We have calculated the pressure dependence of crystal structure in both the phases. Table SI [44] shows a good agreement between the calculated and measured structure of the high-pressure phase at ~4 GPa. The enthalpy calculation as a function of pressure has been done to investigate the phase transition. The difference in enthalpy (ΔH) of the ambient and high-pressure phase as a function of pressure is shown in Fig. 11(a). We can see that the enthalpy difference below 1.5 GPa is within the numerical accuracy of the calculation; however, ΔH is significantly large above 1.5 GPa and increases with an increase in pressure. The calculation therefore indicates a phase transition at about 1.5 GPa.

In order to understand the nature of the phase transition we have performed the group theoretical analysis of phonons at the zone center and various high-symmetry points in the Brillouin zone. The classification of phonon modes at various high-symmetry points is given as

$$\Gamma(000) = 16\Gamma_1 + 16\Gamma_2 + 17\Gamma_3 + 17\Gamma_4 + 32\Gamma_5 + 34\Gamma_6,$$

$$L(1/2\,1/2\,1/2) = 50L_1 + 50L_2 + 49L_3 + 49L_4,$$

$$M(1/2\,0\,0) = 50M_1 + 50M_2 + 49M_3 + 49M_4,$$

$$A(0\,0\,1/2) = 32A_1 + 32A_2 + 34A_3 + 34A_4 + 16A_5 + 17A_6.$$

Here the Γ_5, Γ_6, A_5, and A_6 modes are double-degenerate modes.

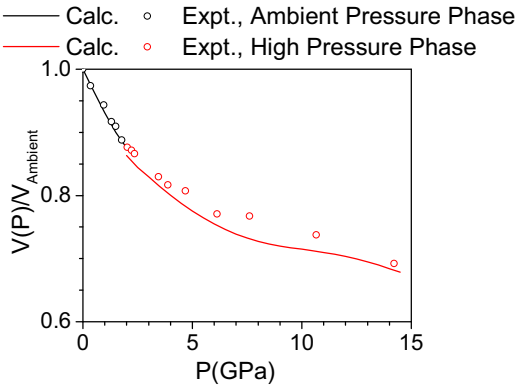

FIG. 12. Calculated and experimental [8] unit-cell volumes of the ambient and high-pressure phases as a function of pressure. The calculated volumes of ambient and high-pressure phases have been normalized with respect to the volume of the ambient phase volume at zero pressure.

We have performed the amplitude mode analysis [45], which indicates that the distortion induced by Γ_1, A_1, L_2, and M_1 [44] phonon modes in the ambient pressure phase would lead to the high-pressure phase transition. We have calculated the structural distortion between the ambient and high-pressure phase structure as a function of pressure. This pressure-dependent distortion is written in terms of distortions corresponding to the Γ_1, A_1, L_2, and M_1 points in the Brillouin zone [Fig. 11(b)]. The distortion picks up above 1.5 GPa and saturates above 2 GPa. We find that the magnitude of the distortion due to the A_1-point phonon is insignificant.

From the *ab initio* lattice dynamics calculation, we have identified the specific phonon modes that correspond to the distortions noted above. Table SII [44] shows that a linear combination of the distortions corresponding to the Γ_1, L_2, and M_1 points in the Brillouin zone with appropriate weight factors can describe the observed distortion vector at 4 GPa as given in Table SI [44]. We found that the L_2-point phonon mode (1.7 meV at 0 GPa) is the primary distortion mode driving the high-pressure phase transition; however, there is also a significant contribution from Γ_1- (4.0 meV at 0 GPa) and M_1- (2.3 meV at 0 GPa) point modes. The displacement pattern of the L-point mode of 1.7 meV shows twisting and bending motion of the -Zn-NC-Au-CN-Zn- chain (Fig. 10 and animation in Supplemental Material [44]). All these modes show a large transverse motion of -Zn-NC-Au-CN-Zn- linkage, where Au has a maximum amplitude of vibration (Fig. 10). The difference in the structure of the ambient and the high-pressure phase at 4 GPa is largely attributed to Au, C, and N dynamics. It seems that the large vibrational amplitude of Au atoms along with connected CN units may create the distortion and lower the symmetry of the structure.

In order to confirm the nature of the phase transition, we have calculated the pressure dependence of the volume. We found a small volume drop (~1.2%) at the transition pressure (Fig. 12), suggesting that the transition is of a weak first-order nature, and is in a good agreement with the experimental data [8].

The calculated elastic constants in the ambient pressure phase of $ZnAu_2(CN)_4$ are given in Table III as a function

TABLE III. Calculated elastic constants in the ambient pressure phase of $ZnAu_2(CN)_4$ as a function of pressure.

	Elastic constants (in GPa)					
P (GPa)	C_{11}	C_{33}	C_{44}	C_{66}	C_{12}	C_{13}
0	36.6	126.8	12.1	3.2	29.7	60.6
1.0	31.6	151.5	12	3.2	25.2	58.4
1.5	31.6	161	12.1	3.2	25	57.9
2.0	31.7	166.4	14.1	3.2	25.3	57.3
3.0	33.4	177.2	13.4	3.1	27.3	57.4
4.0	36	187.6	8.9	3	30.3	58.6

of pressure. In Table IV, we have also shown the calculated various Born stability criteria in the ambient pressure phase of $ZnAu_2(CN)_4$ as a function of pressure. We found that one of the Born stability criteria (C_{66}-$P > 0$, which is equivalent to C_{11}-C_{12}-$2P > 0$) is violated above 3 GPa, i.e., the system becomes elastically unstable. It seems that although the phase transition is primarily driven by an L-point soft phonon mode, which usually leads to a second-order transition with a $2 \times 2 \times 2$ supercell, in the present case the structure is close to an elastic instability that leads to a weakly first-order transition.

VII. NEGATIVE LINEAR COMPRESSIBILITY

We have performed the pressure-dependent calculation of the structures in both the phases. The calculated and measured lattice parameter changes with pressure have been compared in Fig. 13. We find that on compression to 1.8 GPa, the a axis contracts by about 10% whereas the c axis expands by about 8%. The NLC behavior as observed along the c axis from the experimental high-pressure measurements [8] is reproduced by the calculations. We have also computed the elastic constants as a function of pressure. We find that the elastic compressibilities along various crystallographic axes are highly anisotropic and show large positive and negative values along the a- and c axes, respectively ($K_a = 62.7\ \mathrm{TPa}^{-1}$, $K_c = -52.1\ \mathrm{TPa}^{-1}$), which is in close agreement with the experimental values [8].

The origin of NLC can be understood by looking at the elastic compliance matrix (Table II). The elastic compliances along the a axis (s_{11}) and also the c axis (s_{33}) are positive, and

TABLE IV. Calculated Born stability criteria in the ambient pressure phase of $ZnAu_2(CN)_4$ as a function of pressure. For an elastically stable hexagonal crystal, all four Born criteria (elastic constants equations) must be positive.

	Born stability criteria		
P (GPa)	$(C_{44} - P)$	$(C_{66} - P)$	$(C_{33} - P)(C_{11} + C_{12}) - 2(C_{13} + P)^2$
0	12.1	3.2	1062
1.0	11	2.2	1492
2.0	12.1	1.2	2338
3.0	10.4	0.1	3278
4.0	4.9	−1	4335

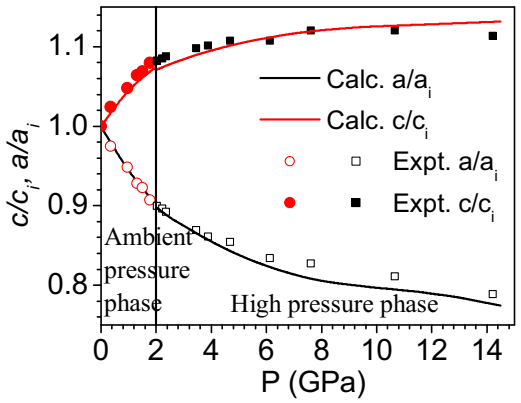

FIG. 13. Calculated and measured [8] change in lattice parameters with pressure in the ambient and high-pressure phases of $ZnAu_2(CN)_4$. The high-pressure structural unit cell is a $2 \times 2 \times 2$ supercell of the ambient pressure phase. $a_i = a_0(2a_0)$ and $c_i = c_0(2c_0)$ are for the ambient (high-) pressure phase. a_0 and c_0 are the lattice constants of ambient pressure phase at 0 GPa.

the shear compressibility s_{13} is large negative and comparable with s_{33}. This indicates that the a axis will contract, but the c axis is elongated with increasing pressure. Another shear compliance component s_{12} is also significantly negative. Interestingly, this indicates that the effect of compression along the a axis will also elongate the b axis but with a reduced magnitude in comparison to the c-axis elongation. As pressure increases, the magnitude of s_{13} decreases while that of s_{12} increases. This unusual behavior of elastic compliance is attributed to the double-helical structure of $ZnAu_2(CN)_4$, which gives rise to a very flexible structure in the a-b plane.

VIII. CONCLUSION

We have used inelastic-neutron-scattering experiments and *ab initio* calculations to gain deeper insights into the structure and dynamics of $ZnAu_2(CN)_4$ as a function of temperature and pressure. The calculations of the structure, phonon spectrum, anisotropic thermal expansion, and anisotropic compressibility are in excellent agreement with experimental data. We have identified specific soft phonon features that correlate very well with the anomalous thermal expansion and compressibility exhibited by $ZnAu_2(CN)_4$. The large anisotropy in the elastic compliance matrix, which is attributed to the flexible network and Au bridging, is responsible for the NLC behavior. We have shown that NLC could be another factor in materials which leads to NTE. The large negative shear elastic compliance (s_{13} and s_{12}) and small tensile elastic compliance (s_{33}) are indeed the major factors controlling the NTE behavior in this compound.

We have identified that the known high-pressure transition at about 2 GPa occurs due to softening of an L-point phonon mode and its coupling with a zone-center phonon and an M-point phonon. Further, the ambient pressure phase is found to be close to an elastic instability as revealed from violation of the Born stability criteria, which results in the phase transition being of a weakly first-order nature.

ACKNOWLEDGMENTS

S. L. Chaplot would like to thank the Department of Atomic Energy, India for the award of the Raja Ramanna Fellowship. The Institut Laue-Langevin (ILL) facility, Grenoble, France, is acknowledged for providing beam time on the IN6 spectrometer.

[1] K. Takenaka, Y. Okamoto, T. Shinoda, N. Katayama, and Y. Sakai, Nat. Commun. **8**, 14102 (2017).
[2] W. Cao, Q. Huang, Y. Rong, Y. Wang, J. Deng, J. Chen, and X. Xing, Inorg. Chem. Front. **3**, 856 (2016).
[3] M. K. Gupta, B. Singh, R. Mittal, S. Rols, and S. L. Chaplot, Phys. Rev. B **93**, 134307 (2016).
[4] J. C. Hancock, K. W. Chapman, G. J. Halder, C. R. Morelock, B. S. Kaplan, L. C. Gallington, A. Bongiorno, C. Han, S. Zhou, and A. P. Wilkinson, Chem. Mater. **27**, 3912 (2015).
[5] T. Lan, C. W. Li, J. L. Niedziela, H. Smith, D. L. Abernathy, G. R. Rossman, and B. Fultz, Phys. Rev. B **89**, 054306 (2014).
[6] F. Bridges, T. Keiber, P. Juhas, S. J. L. Billinge, L. Sutton, J. Wilde, and G. R. Kowach, Phys. Rev. Lett. **112**, 045505 (2014).
[7] M. K. Gupta, R. Mittal, and S. L. Chaplot, Phys. Rev. B **88**, 014303 (2013).
[8] A. B. Cairns, J. Catafesta, C. Levelut, J. Rouquette, A. van der Lee, L. Peters, A. L. Thompson, V. Dmitriev, J. Haines, and A. L. Goodwin, Nat. Mater. **12**, 212 (2013).
[9] V. Gava, A. L. Martinotto, and C. A. Perottoni, Phys. Rev. Lett. **109**, 195503 (2012).
[10] R. Mittal, S. L. Chaplot, H. Schober, and T. A. Mary, Phys. Rev. Lett. **86**, 4692 (2001).
[11] T. A. Mary, J. S. O. Evans, T. Vogt, and A. W. Sleight, Science **272**, 90 (1996).
[12] A. van Roekeghem, J. Carrete, and N. Mingo, Phys. Rev. B **94**, 020303 (2016).
[13] M. S. Senn, C. A. Murray, X. Luo, L. Wang, F.-T. Huang, S.-W. Cheong, A. Bombardi, C. Ablitt, A. A. Mostofi, and N. C. Bristowe, J. Am. Chem. Soc. **138**, 5479 (2016).
[14] R. L. Withers, J. S. O. Evans, J. Hanson, and A. W. Sleight, J. Solid State Chem. **137**, 161 (1998).
[15] Y. Yamamura, S. Ikeuchi, and K. Saito, Chem. Mater. **21**, 3008 (2009).
[16] K. W. Chapman, P. J. Chupas, and C. J. Kepert, J. Am. Chem. Soc. **127**, 15630 (2005).
[17] A. L. Goodwin, M. Calleja, M. J. Conterio, M. T. Dove, J. S. O. Evans, D. A. Keen, L. Peters, and M. G. Tucker, Science **319**, 794 (2008).
[18] A. L. Goodwin, D. A. Keen, M. G. Tucker, M. T. Dove, L. Peters, and J. S. O. Evans, J. Am. Chem. Soc. **130**, 9660 (2008).
[19] A. L. Goodwin, D. A. Keen, and M. G. Tucker, Proc. Natl. Acad. Sci. USA **105**, 18708 (2008).
[20] A. L. Goodwin, M. T. Dove, A. M. Chippindale, S. J. Hibble, A. H. Pohl, and A. C. Hannon, Phys. Rev. B **80**, 054101 (2009).
[21] A. L. Goodwin, B. J. Kennedy, and C. J. Kepert, J. Am. Chem. Soc. **131**, 6334 (2009).
[22] S. J. Hibble, G. B. Wood, E. J. Bilbé, A. H. Pohl, M. G. Tucker, A. C. Hannon, and A. M. Chippindale, Z. Kristallogr. **225**, 457 (2010).
[23] R. Mittal, M. Zbiri, H. Schober, E. Marelli, S. J. Hibble, A. M. Chippindale, and S. L. Chaplot, Phys. Rev. B **83**, 024301 (2011).
[24] A. B. Cairns, A. L. Thompson, M. G. Tucker, J. Haines, and A. L. Goodwin, J. Am. Chem. Soc. **134**, 4454 (2012).
[25] J. W. E. Mariathasan, L. W. Finger, and R. M. Hazen, Acta Crystallogr., Sect. B **41**, 179 (1985).
[26] J. Haines, C. Chateau, J. M. Léger, C. Bogicevic, S. Hull, D. D. Klug, and J. S. Tse, Phys. Rev. Lett. **91**, 015503 (2003).
[27] D. R. McCann, L. Cartz, R. E. Schmunk, and Y. D. Harker, J. Appl. Phys. **43**, 1432 (1972).
[28] J. C. Michael, L. G. Andrew, G. T. Matthew, A. K. David, T. D. Martin, P. Lars, and S. O. E. John, J. Phys.: Condens. Matter **20**, 255225 (2008).
[29] W. Li, M. R. Probert, M. Kosa, T. D. Bennett, A. Thirumurugan, R. P. Burwood, M. Parinello, J. A. K. Howard, and A. K. Cheetham, J. Am. Chem. Soc. **134**, 11940 (2012).
[30] A. D. Fortes, E. Suard, and K. S. Knight, Science **331**, 742 (2011).
[31] J. M. Carpenter and D. L. Price, Phys. Rev. Lett. **54**, 441 (1985).
[32] D. L. Price and K. Skold, *Neutron Scattering* (Academic, Orlando, 1986).
[33] V. F. Sears, Neutron News **3**, 26 (1992).
[34] K. Parlinksi, PHONON 5.11 Software, 2003.
[35] G. Kresse and J. Furthmüller, Phys. Rev. B **54**, 11169 (1996).
[36] G. Kresse and J. Furthmüller, Comput. Mater. Sci. **6**, 15 (1996).
[37] G. Kresse and D. Joubert, Phys. Rev. B **59**, 1758 (1999).
[38] M. Zhang, H. Xu, E. K. H. Salje, and P. J. Heaney, Phys. Chem. Miner. **30**, 457 (2003).
[39] J. P. Perdew, K. Burke, and M. Ernzerhof, Phys. Rev. Lett. **77**, 3865 (1996).
[40] J. P. Perdew, K. Burke, and M. Ernzerhof, Phys. Rev. Lett. **78**, 1396 (1997).
[41] K. Jiří, R. B. David, and M. Angelos, J. Phys.: Condens. Matter **22**, 022201 (2010).
[42] J. Klimeš, D. R. Bowler, and A. Michaelides, Phys. Rev. B **83**, 195131 (2011).
[43] E. Grüneisen and E. Goens, Z. Phys. **29**, 141 (1924).
[44] See Supplemental Material at http://link.aps.org/supplemental/10.1103/PhysRevB.96.214303 for details of calculated phonon dispersion relations, calculated structure, and distortion of $\Gamma 1$, $L2$, and $M1$ phonon modes at 4 GPa and animation of low-energy modes at ambient pressure.
[45] http://www.cryst.ehu.es/.